nature neuroscience

SUPPLEMENTARY INFORMATION

https://doi.org/10.1038/s41593-020-0641-7

In the format provided by the authors and unedited.

Conservation of brain connectivity and wiring across the mammalian class

Yaniv Assaf[1,2], Arieli Bouznach[3], Omri Zomet[4], Assaf Marom[5] and Yossi Yovel[2,6,7]

[1]School of Neurobiology, Biochemistry and Biophysics, The George S. Wise Faculty of Life Sciences, Tel Aviv University, Tel Aviv, Israel. [2]Sagol School of Neuroscience, Tel Aviv University, Tel Aviv, Israel. [3]Kimron Veterinary Institute, Beit-Dagan, Israel. [4]School of Computer Sciences, Sackler Faculty of Exact Sciences, Tel Aviv University, Tel Aviv, Israel. [5]Rappaport Faculty of Medicine, Technion – Israel Institute of Technology, Haifa, Israel. [6]School of Zoology, The George S. Wise Faculty of Life Sciences, Tel Aviv University, Tel Aviv, Israel. [7]The Steinhardt Museum of Natural History, National Research Center for Biodiversity Studies, Tel-Aviv University, Tel Aviv, Israel. e-mail: assafyan@tauex.tau.ac.il; yossiyovel@gmail.com

Supplementary Material

(A) Figures

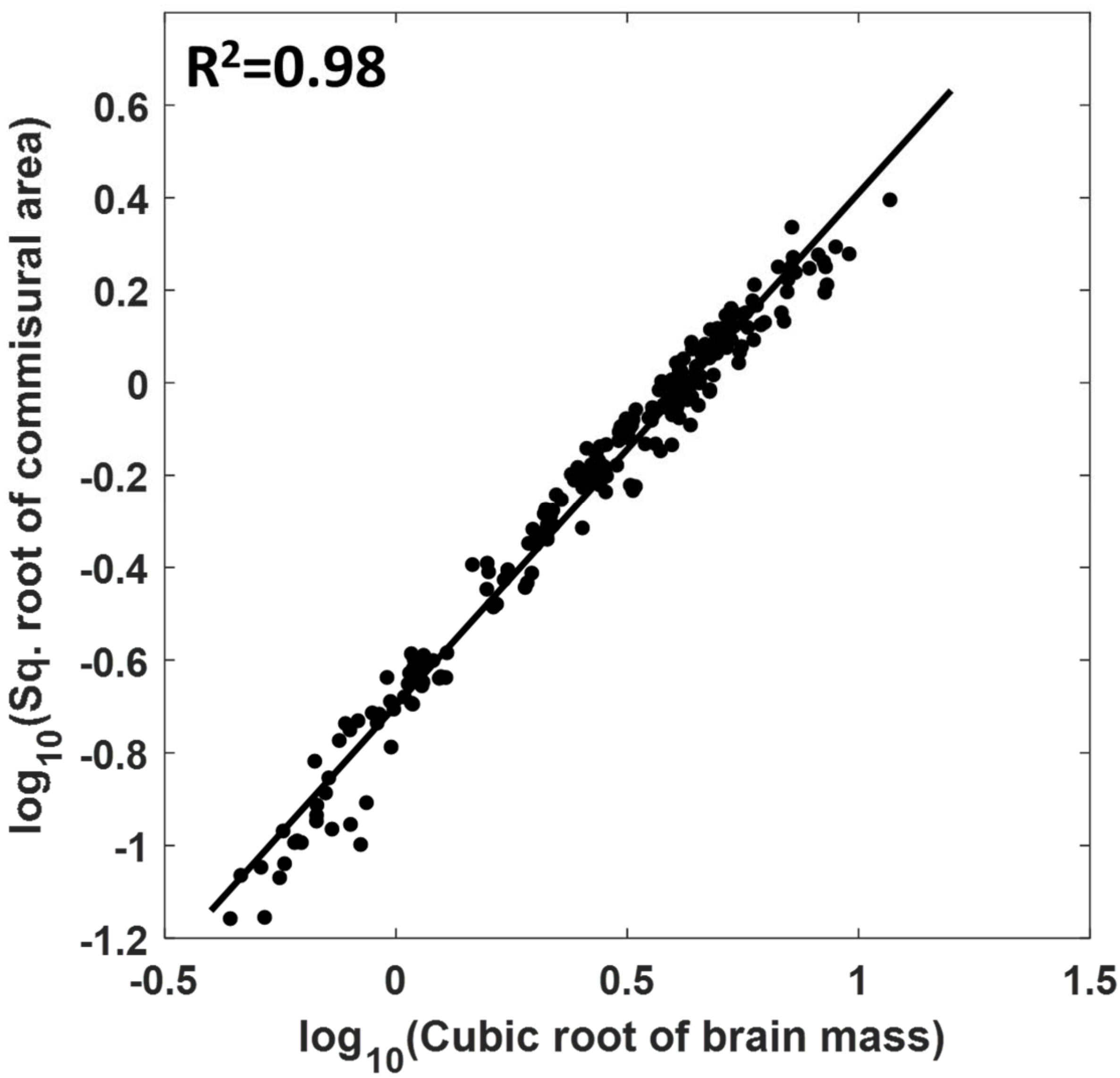

Supplementary Figure 1. Commissural cross section area vs brain volume. Our results replicate previous anatomic results [9].

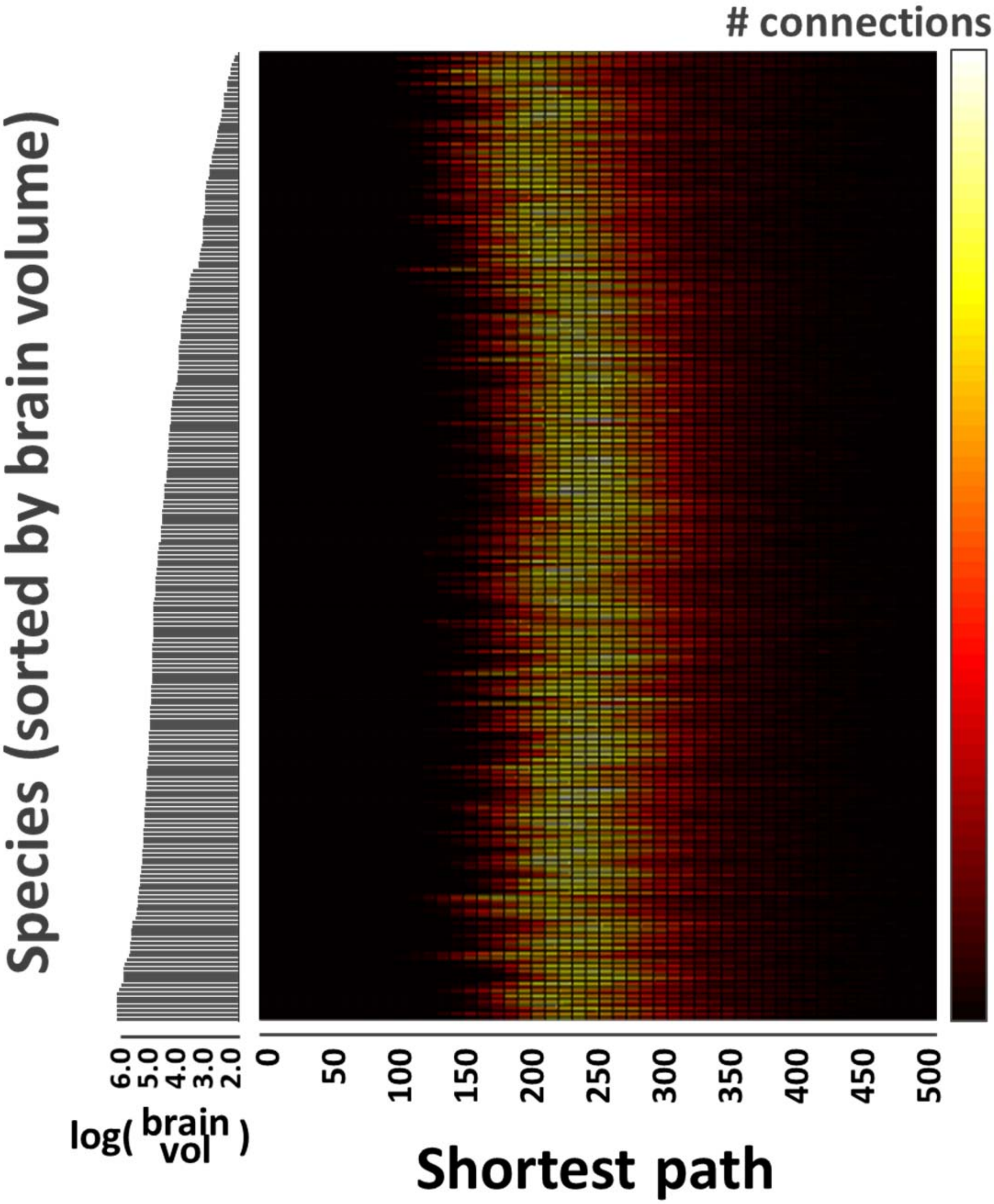

Supplementary Figure 2. Shortest path (SP) distributions. The distributions of shortest paths for all brains sorted by brain volume (indicated by the bars on the y axis). The distribution is very similar across mammals.

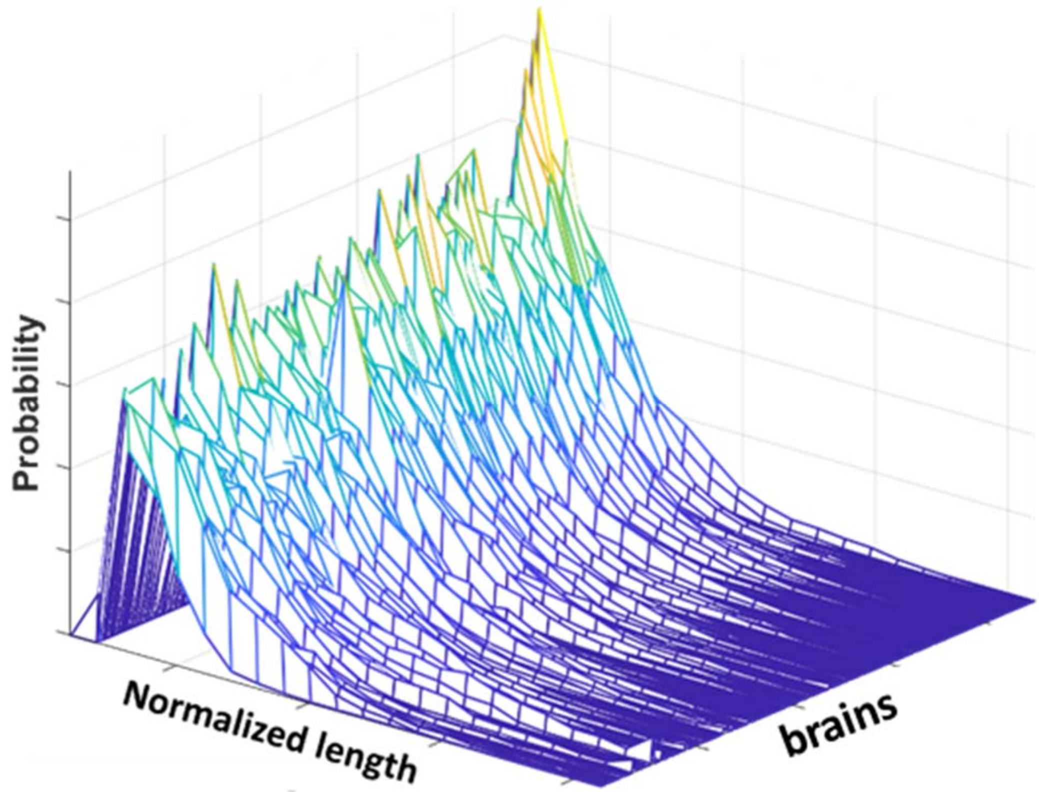

Supplementary Figure 3. Normalized connection length distribution of all brains (sorted according to brain size). Lengths were normalized to brain size by normalizing the voxel size to brain volume (Methods). The figure shows the distribution of lengths for all 123 brains (ordered by brain volume). Note that the length distribution of the brain is strongly skewed to the left unlike in a random network ([11] and Avena-Koenigsberger, A., Misic, B. & Sporns, O. Communication dynamics in complex brain networks. *Nat Rev Neurosci* **19**, 17-33 (2017)).

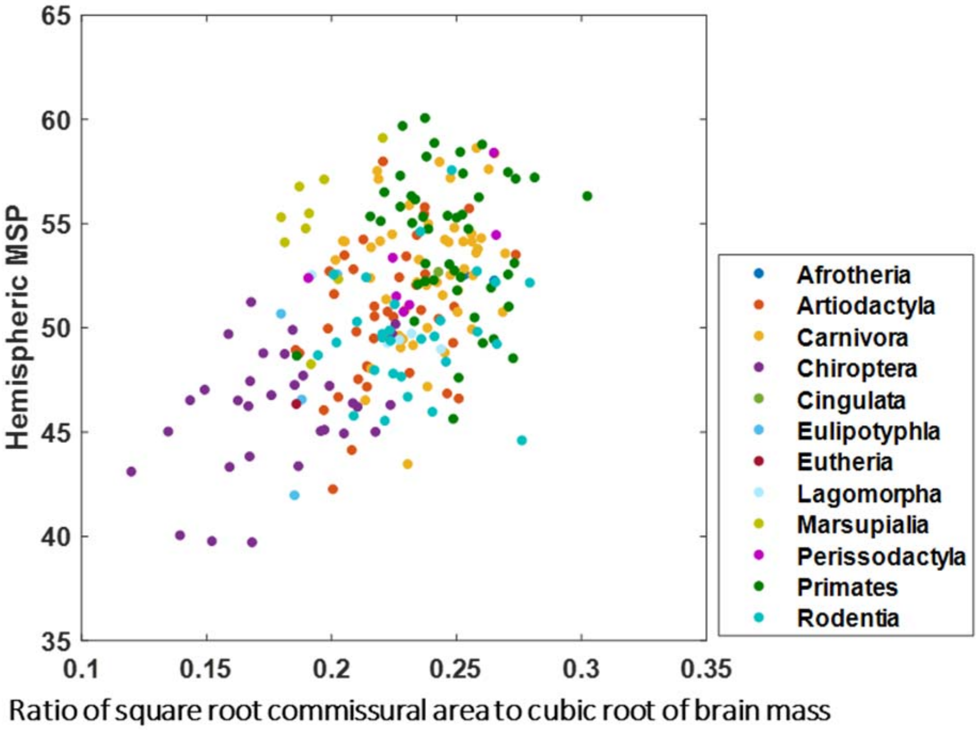

Supplementary Figure 4. Hemispheric MSP as a function of the proportion of commissural connections. The proportion of commissural connections was estimated by dividing the square root of the commissural cross section by the cubic root of brain volume. Unlike in the main figure 2, here we do not use fiber tracking to estimate the proportion of commissural connections but only area measurements, so our result is independent of the parameters of the tracking algorithm. R^2=0.24 (Pearson correlation t-test, $p<10^{-13}$, N=232). All statistical analysis in this figure were two-tailed.

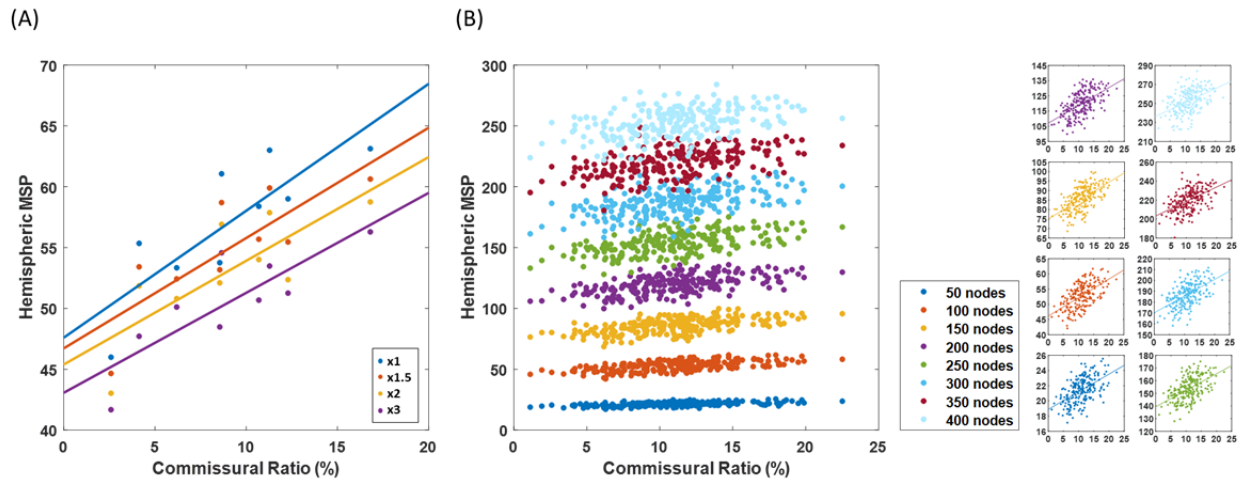

Supplementary Figure 5. Our result was invariant to different scanning and parcellating parameters. (A) The MRI scanning resolution did not affect the conservation principle. The intra-hemispheric MSP is presented as a function of the commissural ratio (as in main Figure 2) for different scanning resolutions (different colors). Nine species (see Methods) were scanned with a higher resolution than the original one (blue). We then reduced the resolution by down-sampling the images. Note that the relation between MSP and commissural ratio is preserved. **(B1)** The number of nodes the brain was parcellated into did not affect the conservation phenomenon. The intra-hemispheric MSP is presented as a function of the commissural ratio (as in main Figure 2) for different brain parcellations. **(B2)** The same as in B1, but here the graph for each number of nodes is presented in its relevant dynamic range (i.e., Y-axes are different).

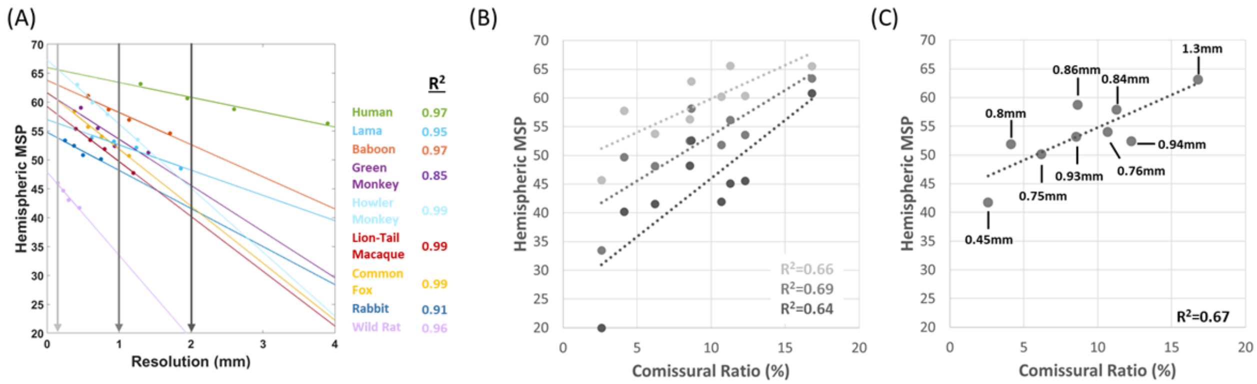

Supplementary Figure 6. The effect of resolution on MSP. The down-sampled resolution dataset shown in Supplementary Figure 5A, was further used to find a linear relation between MSP and scanning resolution. (A) For each of the nine species (N=9, one sample per species, resampled at 4 different resolutions)**, the hemispheric MSP is plotted against** four scanning resolutions. A linear regression was fit for each species. We next used the linear regression model to estimate the expected MSP for three specific resolutions indicated by the gray lines: 0.15mm, 1mm and 2mm. The results of this analysis are shown in (B) where the estimated hemispheric MSP to commissural ratio plot is shown for three resolutions (for the same nine species as in A) and the relation is always highly significant. (C) We used another approach to compare brains with similar scanning resolution. For each of the nine species in (A) we chose the resolution closest to the largest brain (human). This allowed us to reduce the resolution differences between species from a factor of more than 10 to about ~2. Again, the relation between hemispheric MSP and commissural ratio remains highly significant indicating that our observations cannot be a confound of acquisition resolution.

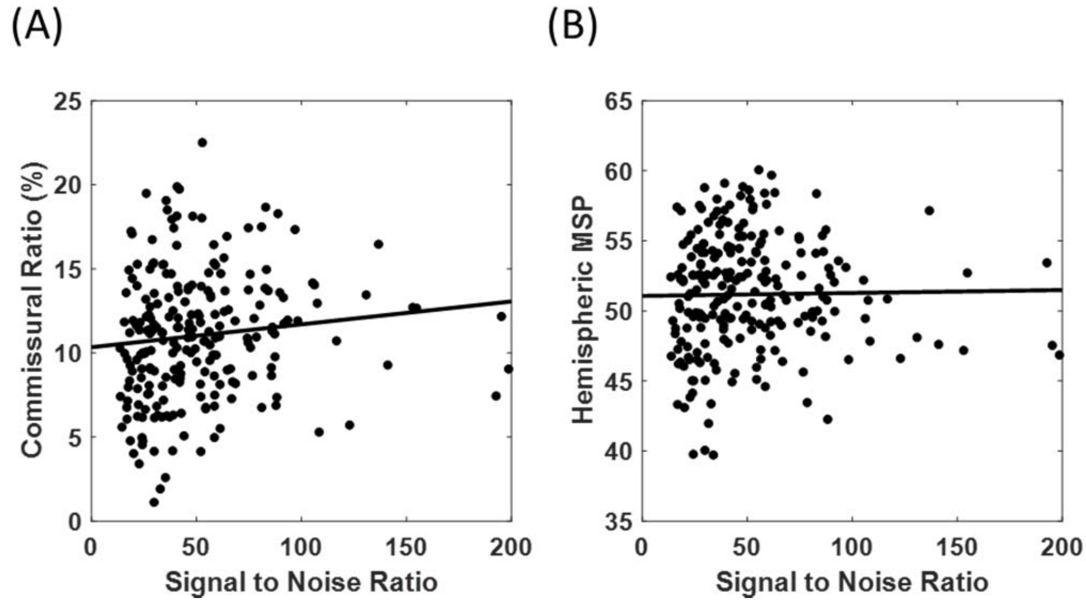

Supplementary Figure 7. Scanning SNR had no effect on the hemispheric MSP (right) or the proportion of commissural fibers (left).

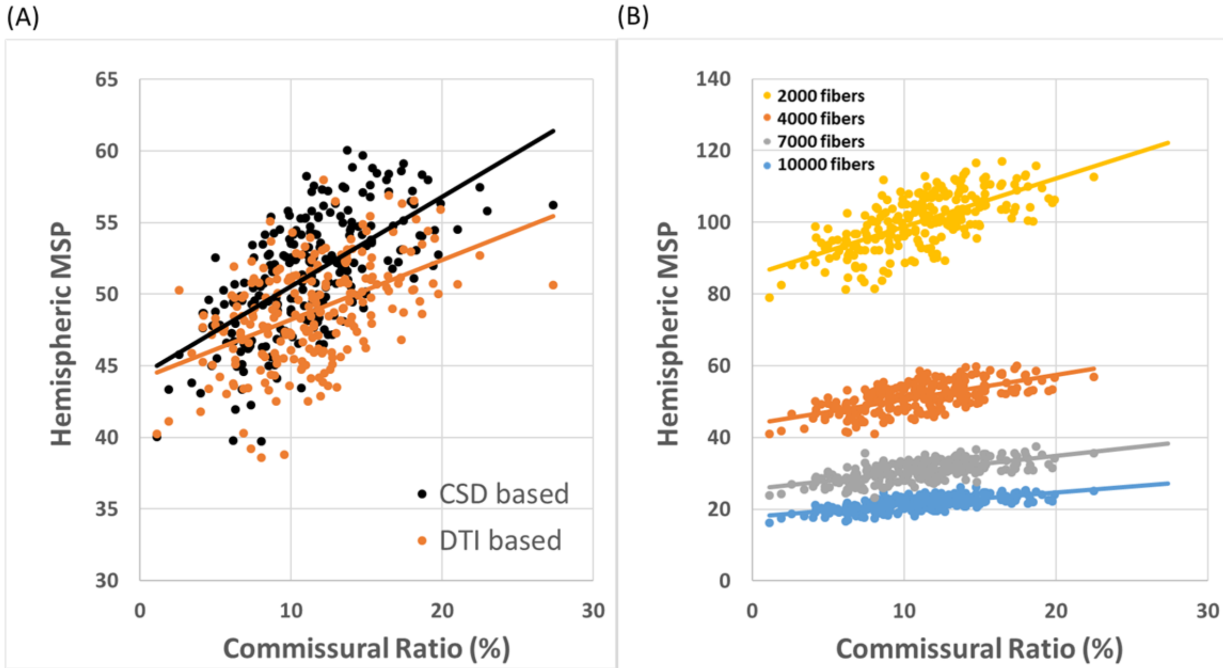

Supplementary Figure 8. Dependency of HMSP on commissural ratio as a function of different tractography parameters. (A) Comparison between CSD and DTI based tracking (see methods). In both tracking procedures significant correlation was found (R^2=0.40 for CSD, black circles and R^2=0.23 for DTI, orange circles, $p<10^{-8}$, Pearson Correlation t-test, N=232 for both analyses). Note that the better correlation for CSD may stem from better coverage of fiber population due to sub-pixel fiber orientations estimation. (B) Dependency of the HMSP vs. commissural ratio as a function of number of sampled fibers. For all comparisons, significant correlation was found (R^2~0.4, Pearson Correlation t-test, $p<10^{-8}$, N=232 for all four analyses). indicating that our observations were independent on the number of fibers that were randomly selected. All statistical analysis in this figure were two-tailed.

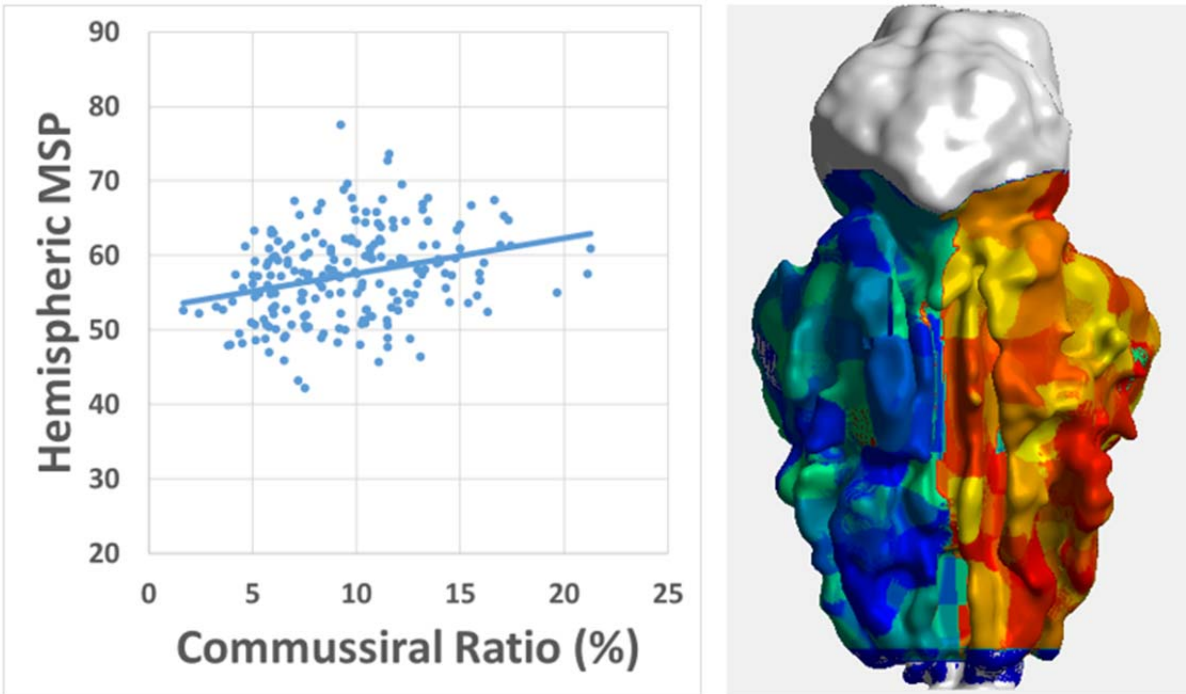

Supplementary Figure 9. Node definition. In our analysis we used the k-means algorithm to cluster the end points of the fiber tracks which were then used as the nodes of the connectome. To validate that this method did not generate the main phenomenon that we describe, we ran the same analysis again, but this time segmenting the cortical surface to patches with similar area and defining each patch as a node (as is often done). (A) This analysis revealed the same relation between hemispheric MSP and commissural ratio as with the k-means approach. (B) An example of the equal-area surface patching method applied on the hyrax brain. The main disadvantage of the k-means based approach was that with the alternative procedure, in some of the small brain, the cortical surface was too small to create big segments which in-turn resulted in connectomes where parts of the nodes are un-connected. Using the k-means clustering approach solved this problem.

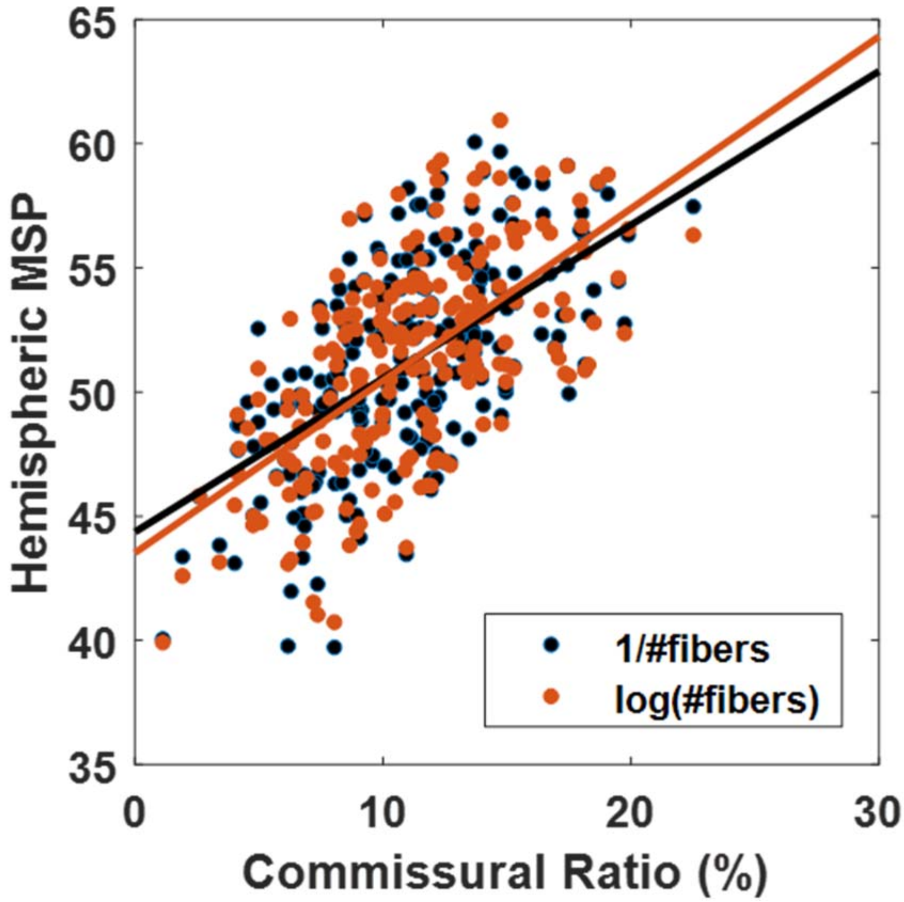

Supplementary Figure 10. Hemispheric MSP (HMSP) as a function of the commissural ratio. This figure is the same as main figure 2) but presented here for two different weightings of the edges – in black, the original (1/#number of fibers) weighting (like in figure 2) and in orange the weighting of an edge is proportional to – log(#number of fibers), where the number of fibers were first normalized between 0-1.

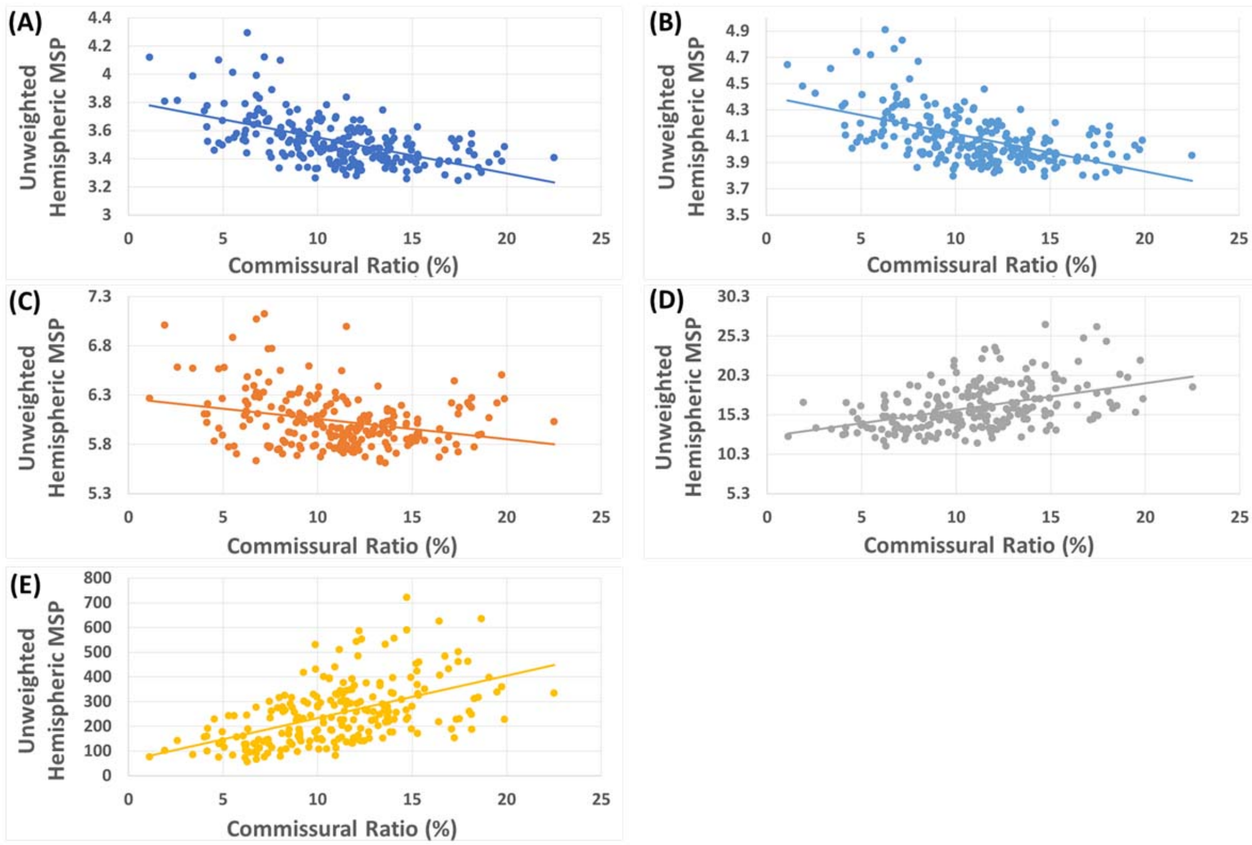

Supplementary Figure 11. Hemispheric MSP as a function of the commissural ratio for the un-weighted network. Each of the plots presents the result for an unweighted network trimmed by an increasing level of trimming (connection strength>0 (A), >2 (B), >5 (C), >10 (D) and >20 (E)).

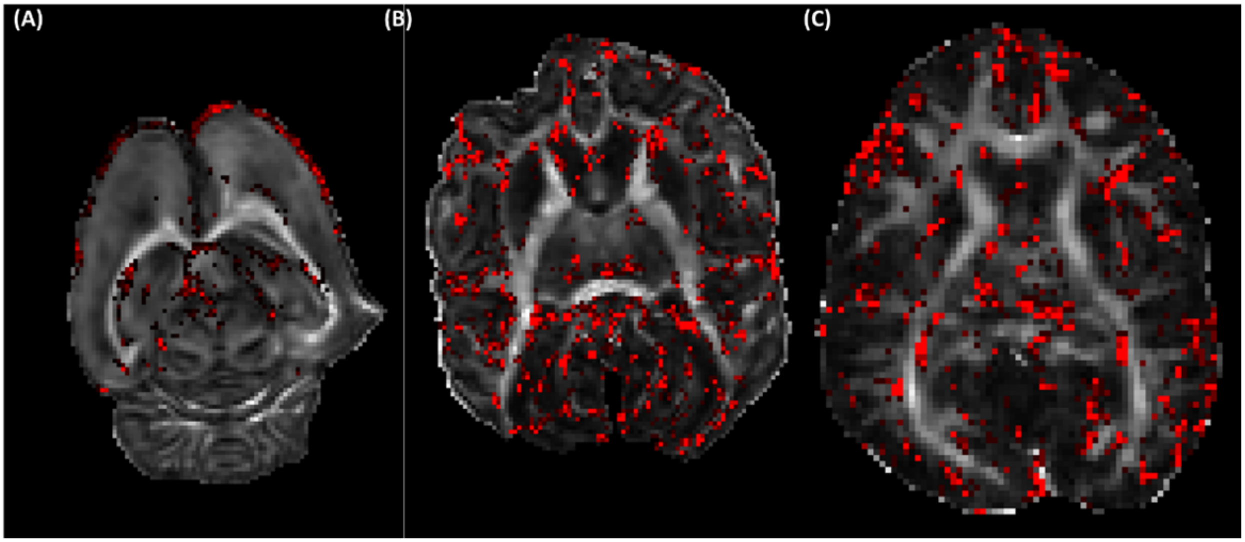

Supplementary Figure 12. Fiber tracking end-pixels. The vast majority of fiber-tracks end points reside in the cortical or sub-cortical gray matter or in close proximity to it. Such analysis is shown for (A) rat, (B) macaque and (C) chimpanzee

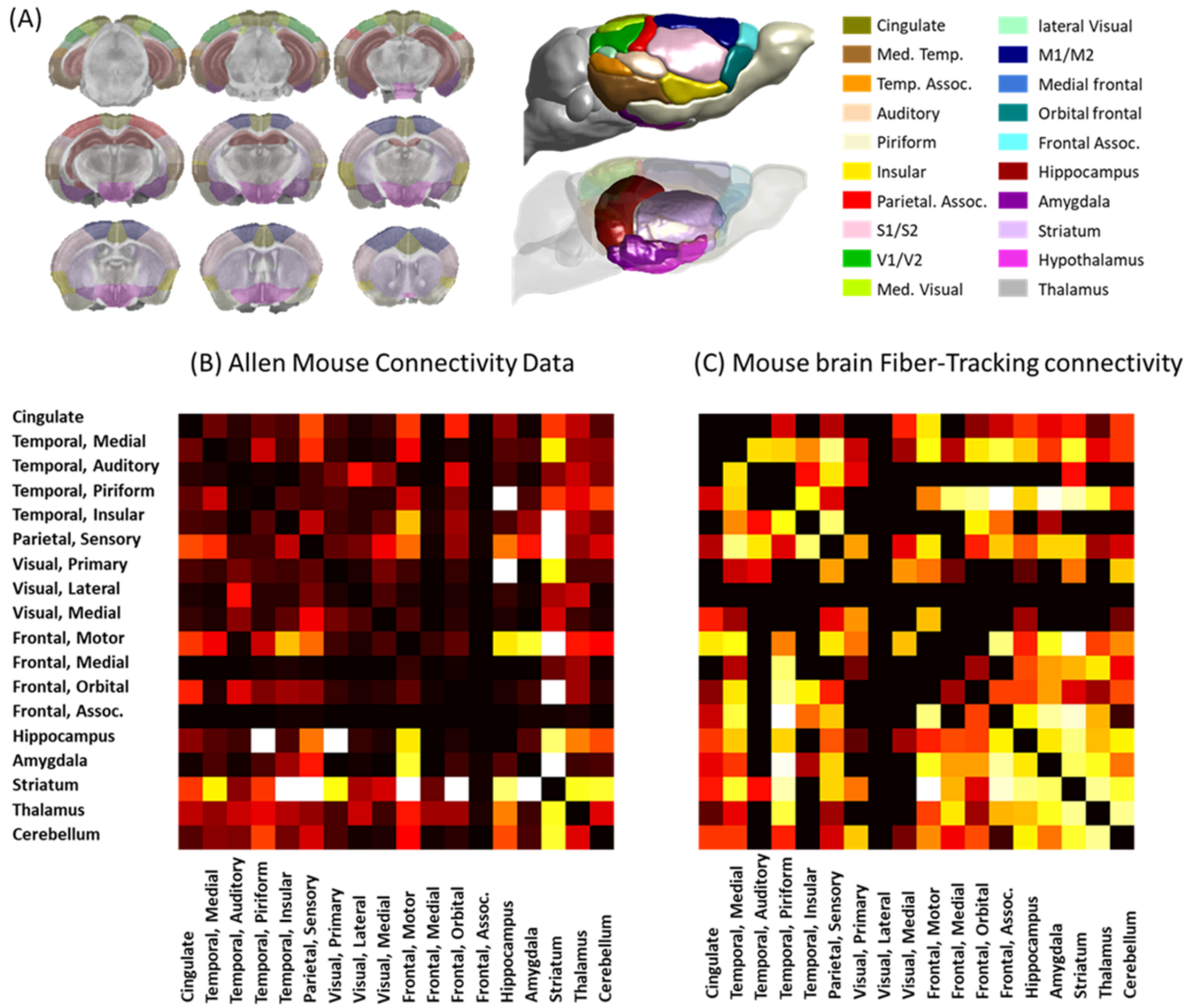

Supplementary Figure 13. Comparing tractography and tract-tracing based connectomes. To examine the validity of the DTI-based connectome acquisition protocol, we compared the Allen mouse connectivity data (formed by tract-tracing) to a tractography based mouse connectome (N=1). (A) To allow this comparison, both data had to be aligned to the same atlas coordinate system where the cortex and sub-cortex are segmented into 20 neuroanatomical regions. (B) and (C) show the corresponding aligned connectomes for the Allen data and our diffusion based tractography, respectively. While the two connectome shows different weights of connection, the general pattern of connectivity is similar as confirmed by a mantel test for comparing matrices which was highly significant ($P=2.3x10^{-4}$, for the comparison of the two matrices) indicating a high correlation between the two matrices.

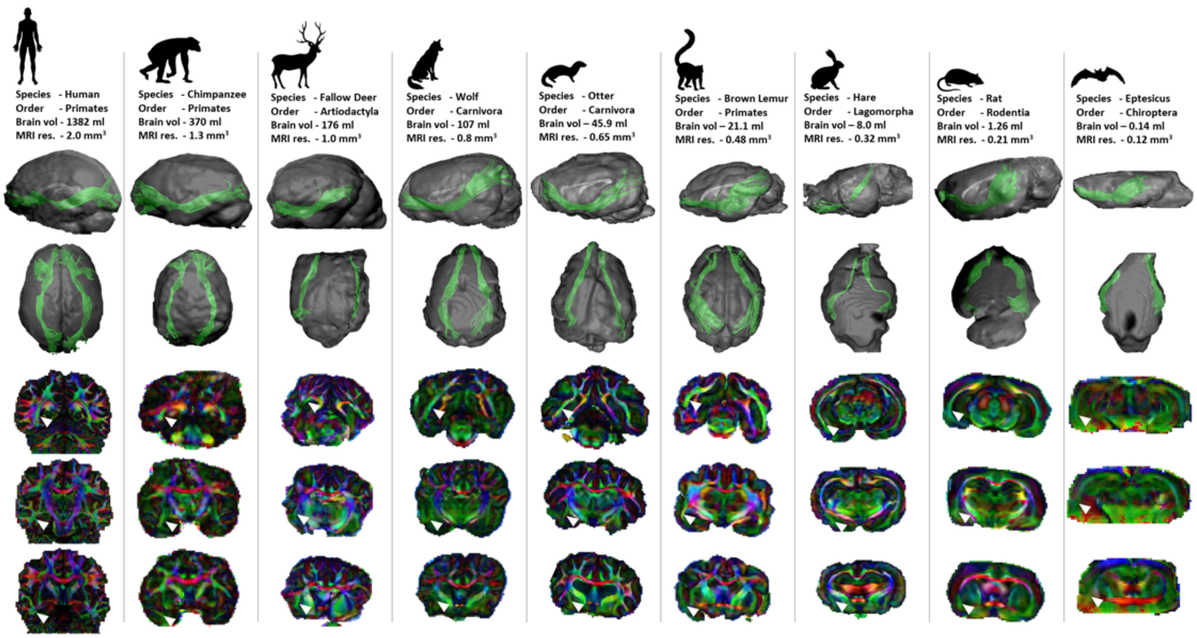

Supplementary Figure 14. The posterior anterior longitudinal system tracts are presented for 10 species spanning the entire range of brain volumes in this study, demonstrating how fiber systems are reconstructed across species independently of scanning resolution. In the color-coded diffusion orientation images, the posterior anterior longitudinal fiber systems are visualized as a green structure at the sides of the anterior commissure, external capsule, claustrum and the hippocampus (see white arrows).

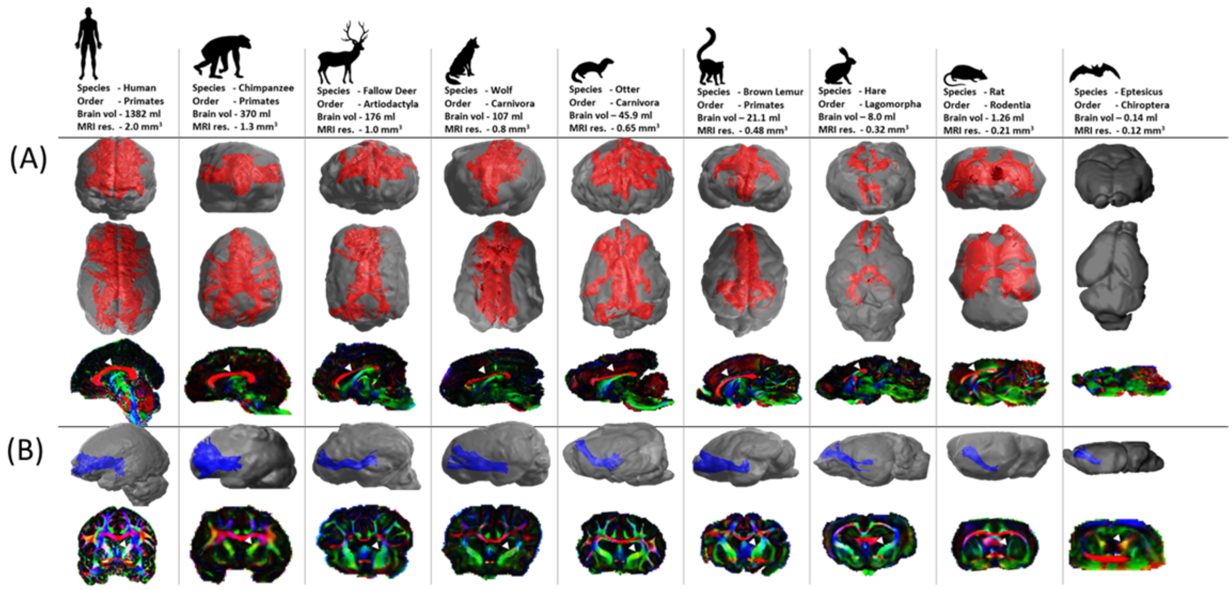

Supplementary Figure 15. The corpus callosum (A) and anterior thalamic radiation (B) are presented for 9 species spanning the entire range of brain volumes in this study, demonstrating how fibers systems are reconstructed across species independently of scanning resolution. In the color-coded diffusion orientation images, the corpus callosum is visualized in the mid-saggital plane as large red structure while the anterior thalamic radiation is identified as part of the green structure composing the anterior part of the internal capsule (see arrows)

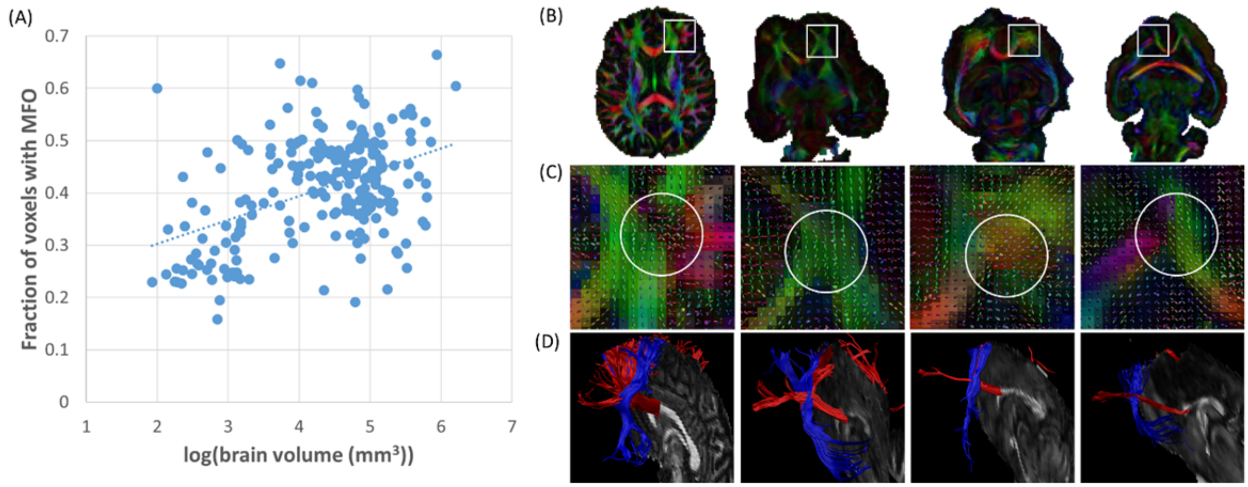

Supplementary Figure 16. Multiple fiber orientation analysis (MFO). Our fiber tracking utilized the spherical harmonics approach to identify MFOs within a voxel. (A) The fractions of voxels with MFO was found to scale with brain volume (R^2=0.19, P<10^{-11}, Pearson Correlation t-test, N=232). (B) We specifically looked for the existence of MFOs at the intersection between the corpus callosum and other longitudinal projections above the forceps minor. We were able to reveal these crossing fibers in all animals, we examined regardless of brain size (human, horse, agouti and hare), see zoom-in (C). (D) reconstruction of the fibers passing through the intersection between the corpus callosum (in red) and thalamic radiation (in blue) that crosses adjacent to forceps minor. Please note that this crossing fibers area can be found in all animals that were inspected. All statistical analysis in this figure were two-tailed.

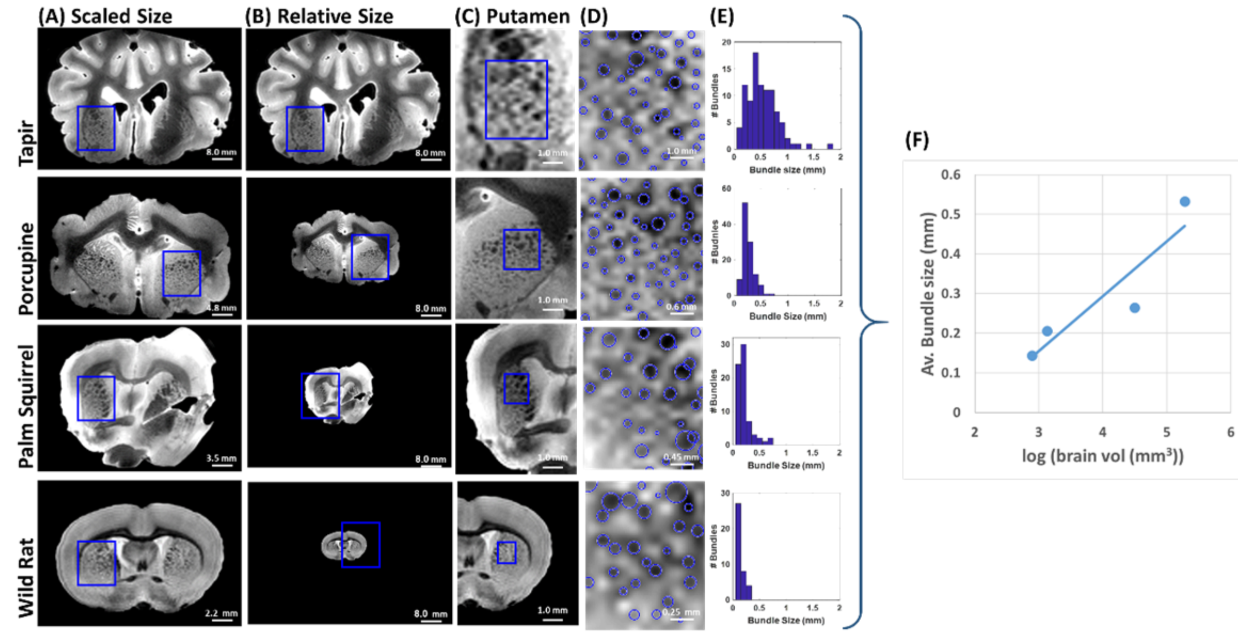

Supplementary Figure 17. Bundle size analysis. (A) and (B) High resolution T2-weighted MRI of four species: Tapir, Porcupine, Palm-Squirrel and Wild Rat are shown in non-equal and equal scales, respectively. (C) The putamen region in each of the animals on a comparative scale shows bundles of white matter (low signal fragmented dots) passing through the putamen area. Evidently, from (C) the size of the bundles scales with brain size as they appear smaller when brain size reduces. Enlargement of the putamen area (D) combined with morphological analysis to reveal the size of these white matter bundles (using imfindcircles function in matlab) allows to quantify the diameter of these bundles (E). The histograms in (E) shows that the distribution of bundle diameters become smaller as brain volume reduces. (F) Correlation between log of brain volume and average bundle size reveals a linear relation (R^2=0.89, Pearson Correlation t-test, p=0.04, N=4). All statistical analysis in this figure were two-tailed.

(B) Supplementary Table 1: List of animals

#	Common Name	Order	Family	Genus	Species	n
1	Addax	Artiodactyla	Bovidae	Addax	A. nasomaculatus	1
2	Cow	Artiodactyla	Bovidae	Bos	B. taurus	1
3	Domestic goat	Artiodactyla	Bovidae	Capra	C. aegagrus	3
4	Nubian ibex	Artiodactyla	Bovidae	Capra	C. nubiana	4
5	Wilderbeest (gnu)	Artiodactyla	Bovidae	Connocheates	C. taurinus	1
6	Thomson’s gazelle	Artiodactyla	Bovidae	Eudorcas	E. thomsonii	1
7	Mountain gazelle	Artiodactyla	Bovidae	Gazella	G. gazella gazella	2
8	Dik-dik	Artiodactyla	Bovidae	Madoqua	M. kirkii	1
9	Oryx	Artiodactyla	Bovidae	Oryx	O. leucoryx	3
10	Domestic sheep	Artiodactyla	Bovidae	Ovis	O. aries	1
11	Llama	Artiodactyla	Camelidae	Lama	L. glama	2
12	Chital (spotted deer)	Artiodactyla	Cervidae	Axis	A. axis	2
13	Bactrian deer	Artiodactyla	Cervidae	Cervus	C. elaphus bactrianus	2
14	Fallow deer	Artiodactyla	Cervidae	Dama	D. dama	3
15	Indian hog deer	Artiodactyla	Cervidae	Hyelaphus	H. porcinus	1
16	Stripped dolphin	Artiodactyla	Delphinidae	Stenella	S. coeruleoalba	2
17	Bottlenose dolphin	Artiodactyla	Delphinidae	Tursiops	T. trancatus	1
18	Reticulated giraffe	Artiodactyla	Giraffidae	Giraffa	G. camelopardalis reticulata	3
19	Domestic pig	Artiodactyla	Suidae	Sus	S. scrofa domesticus	2
20	Wild boar	Artiodactyla	Suidae	Sus	S. scrofa	2
21	Pecari	Artiodactyla	Tayassuidae	Pecari	P. tajacu	2

22	Red panda	Carnivora	Ailuridae	Ailurus	A. fulgens	1
23	Domestic dog	Carnivora	Canidae	Canis	C. lupus familiaris	7
24	Gray wolf	Carnivora	Canidae	Canis	C. lupus	3
25	Lycaon	Carnivora	Canidae	Lycaon	L. pictus	3
26	Blanford's fox	Carnivora	Canidae	Vulpes	V. cana	1
27	Common (red) fox	Carnivora	Canidae	Vulpes	V. vulpes	1
28	Fennec fox	Carnivora	Canidae	Vulpes	V. zerda	1
29	Caracal	Carnivora	Felidae	Caracal	C. caracal	1
30	Domestic cat	Carnivora	Felidae	Felis	F. catus	6
31	Jungle cat	Carnivora	Felidae	Felis	F. chaus	1
32	Sand cat	Carnivora	Felidae	Felis	F. margarita	2
33	Persian leopard	Carnivora	Felidae	Panthera	P. pardus tulliana	2
34	Bengal Tiger	Carnivora	Felidae	Panthera	P. tigris	1
35	Mongoose	Carnivora	Herpestidae	Herpestes	H. ichneumon	1
36	Meerkat	Carnivora	Herpestidae	Suricata	S. suricata	5
37	Stripped Hyaena	Carnivora	Hyaenidae	Hyaena	H. hyaena	2
38	Asian small-clawed otter	Carnivora	Mustelidae	Amblonyx	A. cinerea	1
39	European otter	Carnivora	Mustelidae	Lutra	L. lutra	3
40	Honey badger	Carnivora	Mustelidae	Mellivora	M. capensis	1
41	Ferret	Carnivora	Mustelidae	Mustela	M. putorius	4
42	Nasua	Carnivora	Procyonidae	Nasua	N. Nasua	3
43	Himalayan black bear	Carnivora	Ursidae	Ursus	U. thibetanus laniger	1
44	Trident leaf-nosed	Chiroptera	Hipposideridae	Asellia	A. tridens	1

	bat					
45	Great roundleaf bat	Chiroptera	Hipposideridae	Hipposideros	H. armiger	1
46	Common bent-wing bat	Chiroptera	Miniopteridae	Miniopterus	M. schreibersii	1
47	Wrinkle-lipped free-tailed bat	Chiroptera	Molossidae	Chaerephon	C. plicatus	1
48	European free-tailed bat	Chiroptera	Molossidae	Tadarida	T. teniotis	2
49	Jamaican fruit bat	Chiroptera	Phyllostomidae	Artibeus	A. jamaicensis	1
50	Seba's short-tailed bat	Chiroptera	Phyllostomidae	Carollia	C. perspicillata	2
51	Common vampire bat	Chiroptera	Phyllostomidae	Desmodus	D. rotundus	2
52	Little yellow-shouldered bat	Chiroptera	Phyllostomidae	Sturnira	S. lilium	1
53	Lesser short-nosed fruit bat	Chiroptera	Pteropodidae	Cynopterus	C. brachyotis	1
54	Cave nectar bat	Chiroptera	Pteropodidae	Eonycteris	E. spelaea	2
55	Lyle's flying fox	Chiroptera	Pteropodidae	Pteropus	P. lylei	1
56	Egyptian fruit bat	Chiroptera	Pteropodidae	Rousettus	R. aegyptiacus	5
57	Greater horseshow bat	Chiroptera	Rhinolophidae	Rhinolophus	R. ferrumequinum	1
58	Greater mouse-tailed bat	Chiroptera	Rhinopomatidae	Rhinopoma	R. microphyllum	1
59	Big brown bat	Chiroptera	Vespertilionidae	Eptesicus	E. fuscus	2
60	Fish eating bat	Chiroptera	Vespertilionidae	Myotis	M. vivesi	2
61	Geoffroy's bat	Chiroptera	Vespertilionidae	Myotis	M. emarginatus	1
62	Greater mouse-eared bat	Chiroptera	Vespertilionidae	Myotis	M. myotis	1
63	Kuhl's pipistrelle	Chiroptera	Vespertilionidae	Pipistrellus	P. kuhlii	2
64	Big hairy armadillo	Cingulata	Chlamyphoridae	Chaetophractus	C. villosus	1
65	Eastern grey kangaroo	Diprotodontia	Macropodidae	Macropus	M. giganteus	2
66	Red Kangaroo	Diprotodontia	Macropodidae	Macropus	M. rufus	3

67	Red neck wallaby	Diprotodontia	Macropodidae	Macropus	M. rufogriseus	1
68	Koala	Diprotodontia	Phascolarctidae	Phascolarctos	P. cinereus	1
69	Rat Kangaroo (Rufous bettong)	Diprotodontia	Potoroidae	Aepyprymnus	A. rufescens	2
70	Southern white-breasted hedgehog	Eulipotyphla	Erinaceidae	Erinaceus	E. concolor	3
71	Long-eared hedgehog	Eulipotyphla	Erinaceidae	Hemiechinus	H. auritus	1
72	Rock hyrax	Hyrocoidea	Procaviidae	Procavia	P. capensis	2
73	Hare	Lagomorpha	Leporidae	Lepus	L. timidus	1
74	European Rabbit	Lagomorpha	Leporidae	Oryctolagus	O. cuniculus	4
75	Donkey	Perissodactyla	Equidae	Equus	E. africanus	1
76	Grant's zebra	Perissodactyla	Equidae	Equus	E. quagga boehmi	1
77	Horse	Perissodactyla	Equidae	Equus	E. ferus	2
78	Onager	Perissodactyla	Equidae	Equus	E. hemionus	1
79	South American tapir	Perissodactyla	Tapiridae	Tapirus	T. terrestris	2
80	Golden-handed tamarin	Primates	Callitrichidae	Saguinus	S. midas	1
81	Grey-cheeked mangabey	Primates	Cercopithecidae	Lophocebus	L. albigena	1
82	Lion-tailed macaque	Primates	Cercopithecidae	Macaca	M. silenus	1
83	Hemadryas baboon	Primates	Cercopithecidae	Papio	P. hamadryas	5
84	Black and gold howler	Primates	Atelidae	Alouatta	A. caraya	2
85	Pygmy marmoset	Primates	Callitrichidae	Cebuella	C. pygmaea	1
86	Cotton-top tamarin	Primates	Callitrichidae	Saguinus	S. oedipus	2
87	Emperor tamarin	Primates	Callitrichidae	Saguinus	S. imperator	2
88	Wedge-capped capuchin	Primates	Cebidae	Cebus	C. olivaceus	3
89	Common squirrel	Primates	Cebidae	Saimiri	S. sciureus	1

	monkey					
90	African green monkey (grivet)	Primates	Cercopithecidae	Chlorocebus	C. aethiops	2
91	Vervet monkey	Primates	Cercopithecidae	Chlorocebus	C. pygerythrus	1
92	Mantled (colobus) guereza	Primates	Cercopithecidae	Colobus	C. guereza	1
93	Crab eating macaque	Primates	Cercopithecidae	Macaca	M. fascicularis	8
94	Crested black macaque	Primates	Cercopithecidae	Macaca	M. nigra	1
95	Pig-tailed macaque	Primates	Cercopithecidae	Macaca	M. leonina	1
96	Mandrill	Primates	Cercopithecidae	Mandrillus	M. sphinx	2
97	Western lowland gorilla	Primates	Hominidae	Gorilla	G. gorilla gorilla	1
98	Human	Primates	Hominidae	Homo	H. sapiens	6
99	Chimpanzee	Primates	Hominidae	Pan	P. troglodytes	1
100	Sumatran Orangutan	Primates	Hominidae	Pongo	P. abelii	3
101	Siamang	Primates	Hylobatidae	Symphalangus	S. syndactylus	1
102	Common brown lemur	Primates	Lemuridae	Eulemur	E. fulvus	3
103	Ring tailed lemur	Primates	Lemuridae	Lemur	L. catta	2
104	Guinea pig (hairless cavia)	Rodentia	Caviidae	Cavia	C. porcellus	1
105	Patagonian Mara	Rodentia	Caviidae	Dolichotis	D. patagonum	1
106	Capybara	Rodentia	Caviidae	Hydrochoerus	H. hydrochaeris	1
107	Long tailed chinchilla	Rodentia	Chinchillidae	Chinchilla	C. lanigera	1
108	Gunther’s vole	Rodentia	Cricetidae	Microtus	M. guentheri	1
109	Red-rumped agouti	Rodentia	Dasyproctidae	Dasyprocta	D. leporina	2
110	Coypu (nutria)	Rodentia	Echimyidae	Myocastor	M. coypus	1
111	Indian crested porcupine	Rodentia	Hystricidae	Hystrix	H. indica	2

112	Cairo spiny mouse	Rodentia	Muridae	Acomys	A. Cahirinus	1
113	Golden spiny mouse	Rodentia	Muridae	Acomys	A. russatus	1
114	Tristram's jird (merion)	Rodentia	Muridae	Meriones	M. tristrami	1
115	Mouse	Rodentia	Muridae	Mus	M. musculus	1
116	Fat sand rat	Rodentia	Muridae	Psammomys	P. obesus	1
117	Brown Rat	Rodentia	Muridae	Rattus	R. norvegicus	8
118	Common degu	Rodentia	Octodontidae	Octodon	O. degus	1
119	Black-tailed prairie dog	Rodentia	Sciuridae	Cynomys	C. ludovicianus	1
120	Northen palm squirrel	Rodentia	Sciuridae	Funambulus	F. pennantii	1
121	Caucasian squirrel	Rodentia	Sciuridae	Sciurus	S. anomalus	1
122	Blind mole rat	Rodentia	Spalacidae	Spalax	S.	2
123	Common treeshrew	Scandentia	Tupaiidae	Tupaia	T. glis	1
	Summary:	**Orders**	**Families**	**Genus**	**Species**	**Total**
		12	**50**	**101**	**123**	**232**